JACS
JOURNAL OF THE AMERICAN CHEMICAL SOCIETY

ARTICLE

pubs.acs.org/JACS

Colloidal Gallium Indium Oxide Nanocrystals: A Multifunctional Light-Emitting Phosphor Broadly Tunable by Alloy Composition

Shokouh S. Farvid, Ting Wang, and Pavle V. Radovanovic*

Department of Chemistry, University of Waterloo, 200 University Avenue West, Waterloo, Ontario N2L 3G1, Canada

Supporting Information

ABSTRACT: We demonstrate compositionally tunable photoluminescence in complex transparent conducting oxide nanocrystals. Alloyed gallium indium oxide (GIO) nanocrystals with variable crystal structures are prepared by a colloidal method throughout the full composition range and studied by different structural and spectroscopic methods, including photoluminescence and X-ray absorption. The structures and sizes of the GIO nanocrystals can be simultaneously controlled, owing to the difference in the growth kinetics of In_2O_3 and Ga_2O_3 nanocrystals and the polymorphic nature of both materials. Using the synthesized nanocrystal series, we demonstrate the structural and compositional dependences of the photoluminescence of GIO nanocrystals. These dependences, induced by the interactions between specific defect sites acting as electron donors and acceptors, are used to achieve broad emission tunability in the visible spectral range at room temperature. The nature of the photoluminescence is identified as donor−acceptor pair recombination and changes with increasing indium content owing to the changes in the energy states of, and interactions between, donors and acceptors. Structural analysis of GIO nanocrystals by extended X-ray absorption fine structure spectroscopy reveals that In^{3+} occupies only octahedral, rather than tetrahedral, sites in the spinel-type γ-Ga_2O_3 nanocrystal host lattice, until reaching the substitutional incorporation limit of ca. 25%. The emission decay dynamics is also strongly influenced by the nanocrystal structure and composition. The oxygen vacancy defects, responsible for the observed photoluminescence properties, are also implicated in other functional properties, particularly conductivity, enabling the application of colloidal GIO nanocrystals as integrated optoelectronic materials.

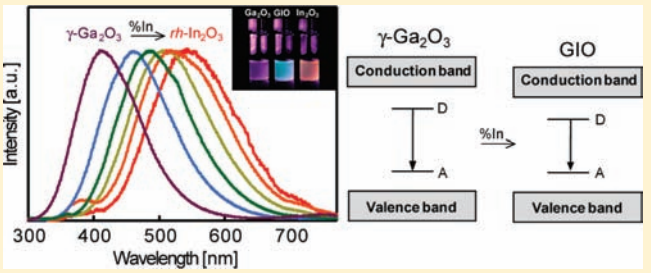

INTRODUCTION

The development of new nanostructured photonic materials and devices, such as light-emitting diodes (LEDs),[1,2] illumination sources,[3−5] photonic crystals,[6] waveguides and lasers,[7−9] has been an active area of chemistry, physics, and materials research. Originally discovered[10] by nearly forgotten Russian scientist Oleg Vladimirovich Losev,[11] LEDs are now becoming increasingly used in flat panel displays, indicators, sensors and as an efficient and convenient replacement of traditional light sources. They have a number of advantages over conventional illumination sources, including lower power consumption, extended lifetime, smaller size, and improved durability and reliability. The design and fabrication of cost-effective LEDs is largely dependent on the development of stable and efficient phosphors with tunable wavelength output. Semiconductor nanocrystal quantum dots have shown much promise as nanoscale emitters for LEDs,[1,2,12] lasers,[8,9] displays,[1] and photoluminescent labels in biomedical applications.[13] Quantum dot photoluminescence (PL) is based on a radiative recombination of an electron in the conduction band and a hole in the valence band, and as such it is size-tunable owing to the quantum confinement effect.[14,15]

Wide band gap semiconductor oxides, often referred to as transparent conducting oxides (TCOs), have found a variety of applications due to their attractive combination of properties—transparency to visible light, hardness, chemical inertness, and electrical conductivity. Such a combination of properties renders their application in the fabrication of transparent electrodes, sensors, catalysts, optical window coatings, and solar cells.[16−19] More recently, TCOs have emerged as candidate materials for multifunctional devices. For example, transparent magnetic semiconductors, obtained by doping TCOs with transition-metal ions, have shown promise in spin-based electronics (spintronics).[20,21] Identification of TCOs with optimal properties and an expansion of their functionalities are therefore research directions of significant current interest. Photoluminescence in TCO nanocrystals (NCs) arises mostly from surface states and localized crystal lattice defects.[22−25] Subsequently, these NCs do not generally experience size-dependent emission tunability associated with quantum confinement, like typical semiconductor quantum dots (i.e., CdSe, CdS, ZnSe, etc.).[14,15] In spite of the technological importance of TCO NCs, the mechanisms of their visible photoluminescence (PL) are still poorly understood, and the control of their optical properties remains a challenge.

Received: December 21, 2010
Published: April 08, 2011

Gallium oxide (Ga_2O_3) is a polymorphic wide band gap ($E_g \approx$ 4.9 eV) material with high n-type conductivity and charge carrier mobility, which originate from the presence of structural defects, particularly oxygen vacancies.[26] Ga_2O_3 occurs in five different allotropic modifications. The stable phase of Ga_2O_3, known as the β-Ga_2O_3 phase, has a monoclinic crystal structure. It is also known that conductive β-Ga_2O_3 containing a high concentration of oxygen vacancies is an efficient blue emitter when irradiated with UV light with energy higher than its band gap.[27] We have shown elsewhere that this luminescence also exists in colloidal metastable γ-Ga_2O_3 NCs with the spinel-type crystal structure and can be tuned in the blue part of the spectrum by controlling their size via the synthesis temperature.[28] Different dopants can also introduce green (beryllium)[29] or red (nitrogen)[5,30] color emission in Ga_2O_3. The origin of these emissions is not well understood or systematically investigated. Unlike bulk materials, NCs can be doped from solution at mild temperatures, allowing for their manipulation using chemical means.[21,31,32] To our knowledge, studies of alloyed colloidal Ga_2O_3 NCs with compositionally tunable emission have not been reported to date. Ga_2O_3 is chemically related to In_2O_3 ($E_g \approx$ 3.7 eV) since both Ga and In belong to the same group of the periodic table and have the same oxidation state in their respective oxides (+3). This should allow for a controlled incorporation of In^{3+} into Ga_2O_3 and Ga^{3+} into In_2O_3 and the formation of colloidal alloyed NCs, without the introduction of new defect sites associated with charge compensation. Furthermore, In_2O_3 is also a polymorph, occurring in the stable cubic phase (bcc-In_2O_3; bcc = body-centered cubic) and the metastable rhombohedral phase (rh-In_2O_3) under the applied synthesis conditions.[33] The fact that both Ga_2O_3 and In_2O_3 are polymorphic materials and have different crystal and electronic structures provides a large number of potential emission-tuning parameters and the possibility of examining the relationship among the size, structure, composition, and emission properties of TCO NCs.

In this paper we report the one-step synthesis of ternary colloidal gallium indium oxide ($Ga_{2-x}In_xO_3$, $0 \le x \le 2$, further in the text generally referred to as GIO) NCs throughout the entire composition range and demonstrate a broad tunability of the visible emission by manipulating the NC composition and structure in solution. The PL mechanism, identified as the donor−acceptor pair (DAP) recombination, changes with the NC composition on the basis of the interactions between donors and acceptors. Substitutional In^{3+} was found to selectively occupy octahedral sites in alloyed GIO NCs with γ-Ga_2O_3 structure. The lifetime of the emission decreases with increasing In concentration in GIO NCs, confirming the structural and compositional dependences of the radiative recombination mechanisms. The reported results open the door for the rational tuning of the visible PL in TCO NCs and further expansion of their inherent degrees of freedom.

EXPERIMENTAL SECTION

Chemicals and Solvents. All reagents are commercially available and were used as received. Gallium acetylacetonate ($Ga(acac)_3$; 99.99%) and indium acetylacetonate ($In(acac)_3$; 98%) were purchased from Strem Chemicals. Oleylamine (70%) and tri-*n*-octylphosphine oxide (TOPO; 90%) were purchased from Sigma-Aldrich Co. Toluene (99.98%, EMD Chemicals), hexane (99.9%, Fischer Scientific), and absolute ethanol were used as solvents without further purification.

Synthesis of GIO Nanocrystals. All reactions were carried out using argon protection. In a typical synthesis, $Ga(acac)_3$ and $In(acac)_3$ were mixed in a 100 mL three-neck round-bottom flask with 9 g of oleylamine and magnetically stirred under a flow of argon at 80 °C until the precursors were fully dissolved. The synthesis of γ-Ga_2O_3 NCs was performed utilizing 1.2 g of $Ga(acac)_3$, and for the syntheses of GIO NCs a certain amount of $Ga(acac)_3$ was systematically replaced with $In(acac)_3$ to obtain alloyed NC samples throughout the full composition range. A solution was degassed and heated to 200 °C (290 °C) at an average rate of ca. 3 °C/min. The reaction mixture was then refluxed in the argon atmosphere for 30 h. The obtained product was cooled to room temperature, and the NCs were precipitated by the addition of 20 mL of ethanol followed by centrifugation at 3000 rpm for 5 min. The isolated white powder was washed three times with ethanol and centrifuged. Finally, NCs were capped with TOPO and dispersed in hexane or toluene.[32]

Measurements and Data Analysis. Nanocrystals were characterized by powder X-ray diffraction (XRD), transmission electron microscopy (TEM), energy-dispersive X-ray (EDX) spectroscopy, and optical absorption. XRD patterns were collected with an INEL powder diffractometer equipped with a position-sensitive detector using monochromatic Cu Kα radiation. TEM imaging and EDX elemental analysis were performed with a JEOL-2010F microscope operating at 200 kV. The specimens were prepared by dropping dilute suspensions of colloidal NCs in toluene on copper grids with lacey Formvar/carbon support films purchased from Ted Pella, Inc. The absorption spectra were collected with a Varian Cary 5000 UV−vis−NIR spectrophotometer.

Photoluminescence spectra were recorded with a Varian Cary Eclipse fluorescence spectrometer. For the delayed PL measurements, the samples were excited in the maximum of the excitation band with a pulsed xenon flash lamp, and the emission intensity at each point was recorded 0.1 ms after excitation (delay time) for 0.04 ms (gate time). Relative quantum yields of the GIO NC samples were calculated using quinine bisulfate (QBS) as the reference substance on the basis of the following expression:

$$\Phi = \Phi_R \frac{I}{I_R} \frac{A_R}{A} \frac{n^2}{n_R{}^2}$$

where Φ is the quantum yield, I is the area under the emission peak (wavelength scale), A is the absorbance at the excitation wavelength, and n is the refractive index of the sample. The subscript R denotes the analogous quantities of the reference. A solution of QBS was prepared in 1 N H_2SO_4 as previously described.[34] The quantum yield of QBS under these conditions was determined to be 0.55.

Indium K-edge X-ray absorption spectroscopy (XAS) measurements were performed at the beamline 06ID-1 at the Canadian Light Source (CLS). The Si(220) crystal was used as an X-ray beam monochromator, and the harmonics rejection was achieved by detuning the second monochromator crystal by 60%. Indium K-edge energy calibration was carried out by using the Sn foil standard (K-edge at 29 200 eV). For GIO NC samples, the spectra were collected in the fluorescence mode with a 32-element germanium array detector. In this setup, the samples were positioned at a 45° angle to the incident beam, while the fluorescence signal was detected at 90° with respect to the incident beam. For In_2O_3 NC samples, the spectra were taken in the transmission mode, and the incident and transmitted X-ray intensities were monitored using ionization chambers. The third ionization chamber was used in conjunction with the Sn foil to provide internal calibration for the In K-edge position. Extended X-ray absorption fine structure (EXAFS) data analysis was performed with the Cherokee and RoundMidnight codes from the Multiplatform Applications for XAFS (MAX) package.[35] EXAFS data were analyzed according to the single scattering theory. First, the background below the edge jump was removed by

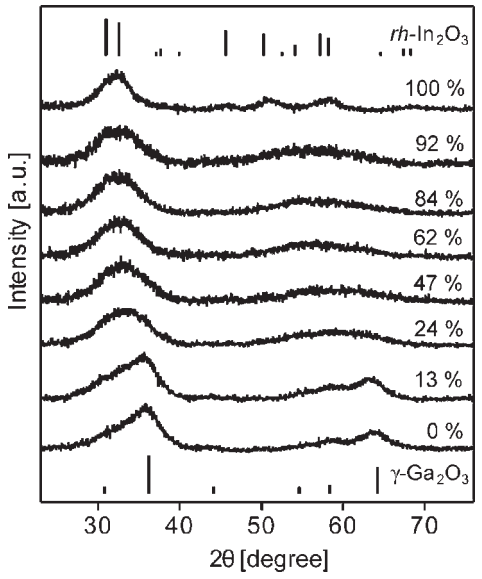

Figure 1. XRD patterns of GIO NCs synthesized with different ratios of $Ga(acac)_3$ and $In(acac)_3$ precursors. The percentages indicate the final concentrations of In. The vertical lines represent XRD patterns of bulk γ-Ga_2O_3 (bottom, JCPDS 20-0426) and rh-In_2O_3 (top, JCPDS 21-0406).

extrapolation of the pre-edge absorption using a linear function, and the postedge background was modeled by interpolation of the atomic-absorption background by a fifth- or sixth-degree polynomial. The extracted EXAFS spectra were converted from energy (E) to wave vector (k) and then Fourier transformed from k-space to R-space by using a Kaiser−Bassel window (τ = 2.5) defined between 2.40 and 10.56 $Å^{-1}$. The peaks corresponding to the first oxygen and second cation shells were filtered and back-Fourier transformed to k-space for further fitting. EXAFS structural parameters, including the coordination number, N, the bond length, R, and the Debye−Waller factor, σ^2, were obtained by least-squares analysis of the Fourier-filtered data using phase and amplitude functions generated from the FEFF6 code[36] (see the Supporting Information) with input data based on the crystallographic information for In−O and metal−metal bond distances.[37−39]

RESULTS AND DISCUSSION

The synthesis conditions were developed and optimized to obtain alloyed GIO NCs with Ga_2O_3 and In_2O_3 crystal structures. All samples were obtained in a high yield, with an average yield of ca. 85%. Figure 1 shows XRD patterns of GIO NCs with different compositions synthesized at 200 °C. The compositions of GIO NCs were determined by EDX spectroscopy and are shown in Figure 1 as the concentration (atom %) of In. The XRD pattern of pure Ga_2O_3 NCs (0 atom % In) matches very well the pattern of metastable γ-Ga_2O_3. Similarly, the NC sample synthesized with $In(acac)_3$ as the only precursor in the reaction mixture (100 atom % In) exhibits a crystal structure characteristic for metastable rh-In_2O_3 (corundum-type In_2O_3).[33] XRD peaks for pure In_2O_3 and Ga_2O_3 NCs are narrower and better defined than those for GIO NCs synthesized under identical conditions, which is consistent with an impurity-induced NC lattice disorder and a decrease in the average NC size, suggesting that the presence of foreign ions inhibits NC growth[31] even for ions that have similar chemical behavior. As the concentration of In in the reaction mixture approaches that of Ga, the formation of GIO

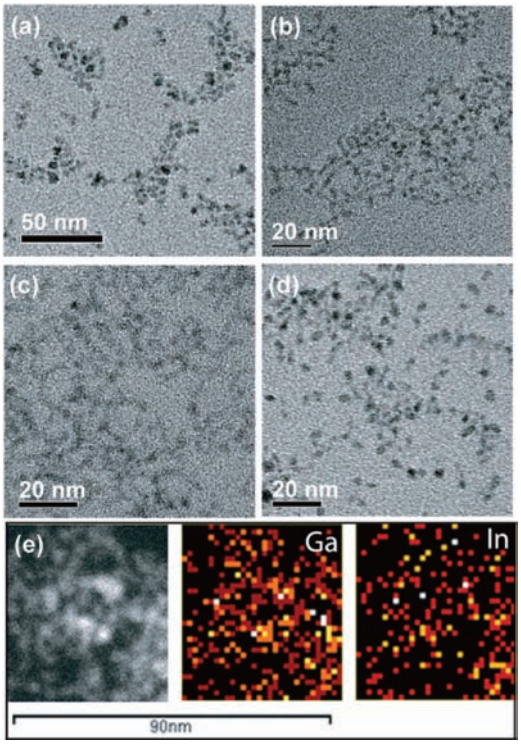

Figure 2. (a−d) TEM images of GIO NCs with (a) 5, (b) 24, (c) 47, and (d) 92 atom % In. (e) Scanning TEM (STEM) image of GIO NCs containing 47 atom % In (left panel) and the corresponding EDX elemental maps of Ga (middle panel) and In (right panel) obtained in the STEM mode.

NCs with rh-In_2O_3 structure, in addition to those with γ-Ga_2O_3 structure, becomes evident. The presence of GIO NCs with rh-In_2O_3 structure can be identified in samples with a final In concentration of ca. 25 atom %, and they become dominant when the In concentration reaches about 50 atom %. In this intermediate composition range GIO NCs with both γ-Ga_2O_3 and rh-In_2O_3 structures can contribute to the PL properties. To study the optical behavior of GIO NCs with respect to their crystal structure and to distinguish PL of the two metastable phases of mixed oxide NCs, we used the difference in kinetics of In_2O_3 and Ga_2O_3 colloidal NC growth. Synthesis of In_2O_3 NCs at high temperatures (ca. 250 °C and above) leads to the formation of larger NCs (≥10 nm in diameter) with bcc-In_2O_3 structure, while at lower temperatures (ca. 200 °C) the slower growth favors the formation of small-sized (ca. 3.5 nm) metastable rh-In_2O_3 NCs (Figure S1, Supporting Information).[33] On the other hand, Ga_2O_3 NCs, which grow or ripen much slower, are stabilized in the γ-Ga_2O_3 phase throughout the same temperature range (Figure S2, Supporting Information).[28] The XRD patterns of GIO NCs synthesized at 290 °C reflect this difference in the kinetics of In_2O_3 and Ga_2O_3 NC growth. The presence of larger In-rich GIO NCs with bcc-In_2O_3 structure is observed in the samples prepared at 290 °C with higher concentrations of the $In(acac)_3$ precursor (Figure S3, Supporting Information). However, NCs with bcc-In_2O_3 structure show negligible emission, and the PL properties of these samples arise only from GIO NCs with γ-Ga_2O_3 structure (vide infra).

Figure 2 shows TEM images of GIO NCs with In contents of 5 (a), 24 (b), 47 (c), and 92 (d) atom %. For similar concentrations of In and Ga, the obtained NCs are somewhat smaller and tend to

dx.doi.org/10.1021/ja111514u |J. Am. Chem. Soc. 2011, 133, 6711–6719

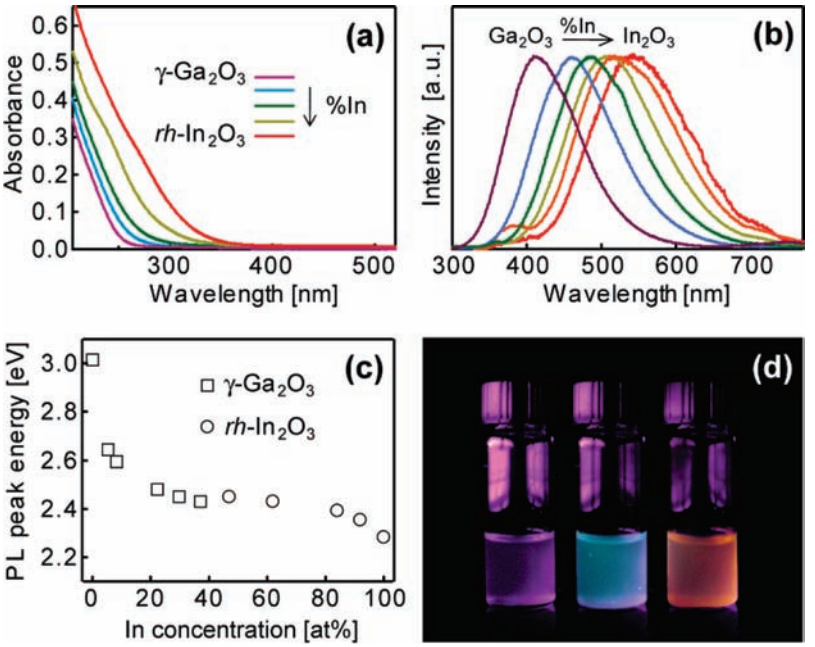

Figure 3. (a) Absorption spectra of GIO NCs with varying In content. (b) Photoluminescence spectra of GIO NCs with 0 (purple), 13 (blue), 24 (green), 47 (olive), 84 (orange), and 100 (red) atom % In synthesized at 200 °C. (c) Photoluminescence peak energies of GIO NCs as a function of the In concentration. Different symbols show the dominant crystal structure of GIO NCs based on XRD data. (d) Photograph of γ-Ga_2O_3 (left), GIO (24 atom % In, middle), and rh-In_2O_3 (right) NCs synthesized at 200 °C.

form a network-like structure, similar to undoped NCs at the early growth stages.[33] This reduction in size is associated with the suppression of the NC growth in the presence of impurity ions[31] and is consistent with the XRD data in Figure 1. The distribution of constituent elements was examined by EDX elemental mapping. Figure 2e shows EDX elemental maps of GIO NCs with 47 atom % In. The images indicate a homogeneous distribution of elements in NCs. This finding was confirmed for other samples regardless of the NC structure.

Absorption spectra of GIO NCs with different compositions are shown in Figure 3a. Ga_2O_3 has a larger band gap than In_2O_3. As the amount of In in GIO NCs increases, the onset of the band gap absorption shifts to longer wavelengths, indicating an electronic structure dependence on the NC composition. Ga_2O_3 is a wide band gap semiconductor with a large effective mass of an electron ($m_e^* \approx 0.34m_0$),[40] and as such its band gap energy is independent of the NC size (Figure S4, Supporting Information).[28] Substitutional incorporation of In into Ga_2O_3 narrows its band gap, leading to a red shift in the band gap absorption. This observation is in agreement with previous findings about alloyed semiconductor NCs.[41] Conversely, GIO NCs having rh-In_2O_3 structure exhibit a higher band gap energy compared to undoped rh-In_2O_3 NCs (red trace in Figure 3a). The electronic band structure is determined by the size of the constituent cations, allowing for band gap and optical property engineering of the NC systems that are not subject to quantum confinement in the experimentally achievable sizes. When excited into the band gap, Ga_2O_3 NCs exhibit a broad PL band with a significant Stokes shift (Figure S5, Supporting Information). A large Stokes shift suggests a localized (non band gap) nature of the PL transition, which is in sharp contrast with a typical excitonic recombination transition in quantum dots.[15] This transition has been assigned to the DAP recombination, where a donor is an oxygen vacancy, and an acceptor is a gallium vacancy or gallium−oxygen vacancy pair.[27,28] The donor−acceptor pairs are formed upon excitation according to the following equation in the Kröger−Vink notation:

$$(V_O, V_{Ga})' + V_O^{\bullet} + h\nu \rightarrow (V_O, V_{Ga})^x + V_O^x$$

The blue emission is described by the reverse process. These DAP PL bands in Ga_2O_3 are characteristically broad and featureless owing to a strong phonon cooperation and possibly broadened distribution of the donor and acceptor energy states.[42,43] The observed PL band red shifts as the concentration of In increases in GIO NCs, reaching the lowest emission energy for pure rh-In_2O_3 NCs (Figure 3b). This composition dependence allows for continuous tuning of the emission throughout most of the visible spectrum, rendering alloyed GIO NCs promising materials for tunable LEDs. The PL peak energy dependence on the NC composition is plotted in Figure 3c. This dependence follows a horizontal sigmoidal shape. The emission energy of GIO NCs initially drops sharply with increasing concentration of In in γ-Ga_2O_3 and then saturates when the In content reaches ca. 30 atom %. Indium-rich GIO NCs with rh-In_2O_3 structure behave as a mirror image with increasing Ga concentration, although with a narrower tuning range (ca. 2.28−2.45 eV). For similar concentrations of both cations the energies of the PL peaks are essentially the same regardless of the NC structure. The color changes from purple for γ-Ga_2O_3 NCs, via different nuances of blue-green for GIO NCs, to orange for rh-In_2O_3 NCs. Figure 3d qualitatively demonstrates the composition-induced tunability of the GIO NC emission and their potential as inorganic LEDs. Importantly, a decrease in NC size leads to a blue shift of the γ-Ga_2O_3 NC emission, which can be associated with an increase in the Coulombic interactions between donors and acceptors due to a decrease in their average separation.[28] However, the emission peaks of GIO NCs are red-shifted for higher In concentrations in

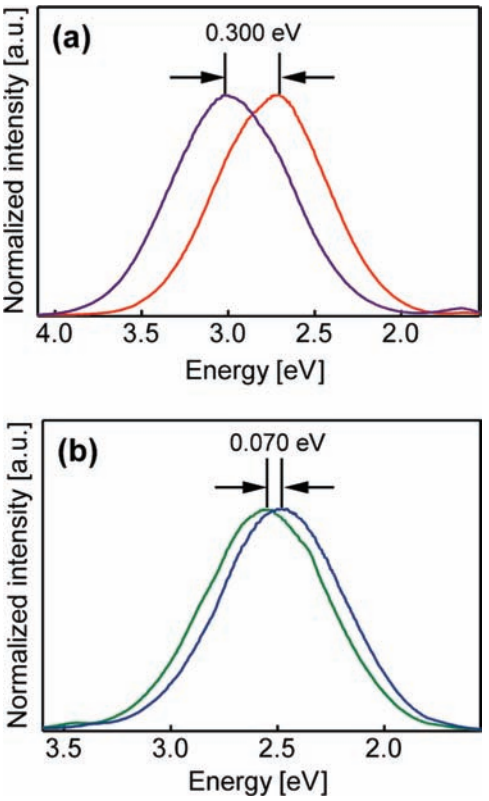

Figure 4. (a) Photoluminescence of 3.3 nm γ-Ga_2O_3 NCs synthesized at 200 °C (purple) and 6.0 nm γ-Ga_2O_3 NCs synthesized at 290 °C (red). (b) Photoluminescence of GIO NCs containing 24 atom % In synthesized at 200 °C (green) and 22 atom % In synthesized at 290 °C (blue).

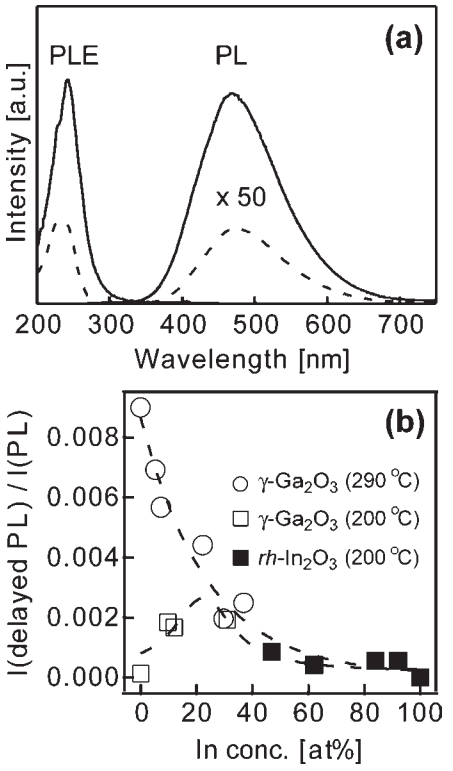

Figure 5. (a) Steady-state (solid line) and delayed (dashed line) PL spectra of GIO NCs containing 5 atom % In. The corresponding excitation (PLE) spectra are shown with the same lines. The delayed PL and PLE spectra were collected 0.1 ms after excitation and are multiplied by a factor of 50 for clarity. (b) Ratio of 0.1 ms delayed PL and steady-state PL intensities of GIO NCs as a function of the In content. The synthesis temperatures and the corresponding majority structures of GIO NCs are indicated in the graph. The exponential and Lorentzian function fits are shown as a guide to the eye.

spite of the fact that In^{3+} ions in solution inhibit NC growth. Figure 4a compares PL spectra of γ-Ga_2O_3 NCs prepared at different temperatures. The blue PL band of γ-Ga_2O_3 NCs synthesized at higher temperature is red-shifted owing to the larger NC sizes and the lower concentration of native defects.[28] The same comparison for GIO NCs having similar compositions (20−25 atom % In) reveals a much smaller difference in the emission energies (Figure 4b). Smaller differences in PL band energies of GIO NCs synthesized at different temperatures indicate that the nature of DAP recombination changes with the incorporation of In into γ-Ga_2O_3 NCs.

Figure 5a compares steady-state (solid line) and delayed (dashed line) PL spectra of GIO NCs containing 5 atom % In. The delayed PL spectrum was collected 0.1 ms after NC excitation through the band gap. The PL and delayed PL spectra, as well as the corresponding excitation (PLE) spectra, have the same structures and band shapes, confirming that at low-to-intermediate In content the observed emission is due to DAP recombination in NCs having the same structure and very similar compositions, rather than subsets of NCs with particular compositions (i.e., Ga-rich and In-rich NCs). The red shift of the delayed relative to the steady-state PL spectrum, which is associated with recombination of more distant donors and acceptors,[28] is much smaller than for pure Ga_2O_3 NCs. This difference suggests stronger delocalization of an electron on a donor in GIO than in Ga_2O_3 NCs. The ratios of delayed PL and PL band intensities are summarized in Figure 5b for different In concentrations in GIO NCs prepared at different temperatures.

To distinguish the influence of the GIO NC structure and composition on the PL decay dynamics, we measured the intensity ratios of delayed and steady-state PL for Ga-rich NCs prepared at 290 °C (open circles) and In-rich NCs prepared at 200 °C (filled squares). As mentioned above, the only detected secondary phase in the synthesis at 290 °C is bcc-In_2O_3-type GIO NCs, which show a negligible emission (Figure S6, Supporting Information). The PL spectra of these samples come from GIO NCs with γ-Ga_2O_3 structure. On the other hand, for the samples synthesized at 200 °C PL is due to NCs with both γ-Ga_2O_3 and rh-In_2O_3 structures, depending on the NC composition. The intensity ratios (delayed PL/PL) for NCs synthesized at 290 °C decrease exponentially with increasing concentration of In (Figure 5b, open circles). These data further suggest a change in the nature of the DAP emission of γ-Ga_2O_3-type NCs with increasing incorporation of In. An interesting comparison is the relationship between delayed and steady-state PL intensities for GIO NCs with γ-Ga_2O_3 structure prepared at 200 °C (Figure 5b, open squares) and 290 °C (open circles). A sharp decrease in the delayed PL intensity is observed for NCs prepared at the lower temperature. This increase in the PL decay rate is associated with shorter donor−acceptor distances in NCs obtained at lower synthesis temperatures.[28] As the concentration of In becomes larger the delayed PL/PL ratio for NCs synthesized at lower temperature approaches that of NCs synthesized at higher temperature.

dx.doi.org/10.1021/ja111514u |J. Am. Chem. Soc. 2011, 133, 6711–6719

The quantum yield values for the samples in Figure 5b are shown in Figure 6. For γ-Ga_2O_3 NCs the quantum yield is ca. 20%, and it drops exponentially with increasing In content. This trend is also consistent with a different nature of PL in alloyed GIO relative to pure Ga_2O_3 and In_2O_3 NCs. The development of LEDs that emit white light has attracted much attention lately for their potential use in the next generation of displays and as lighting sources.[12,44] The broad tunability, large-emission Stokes shifts, and long lifetimes render GIO NC-based phosphors potentially promising materials for the design of white light emitters.

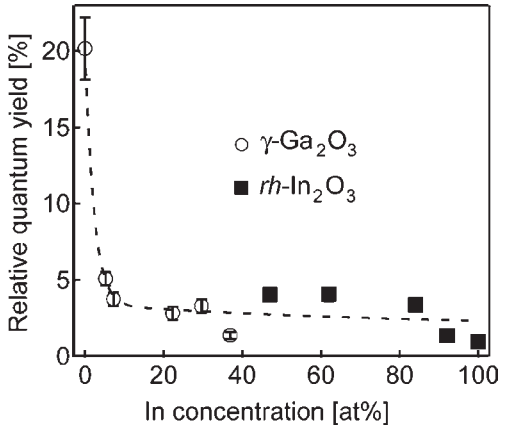

Figure 6. Indium concentration dependence of the relative quantum yield for GIO NCs having different crystal structures as labeled in the graph. The dashed line is an exponential fit to the experimental data points.

To obtain quantitative information about the local environment of In sites, we conducted a systematic XAS study of photoluminescent GIO NC samples having different In concentrations. Normalized In K-edge X-ray absorption spectra of GIO and rh-In_2O_3 NCs in the full spectral range are shown in Figure S7 (Supporting Information). A direct comparison between the spectra of GIO and rh-In_2O_3 NCs in the near-edge region confirms that indium ions are in the +3 oxidation state in GIO NCs. Figure 7a shows the *k*-weighted In K-edge EXAFS spectra of GIO NCs having different compositions, synthesized at 200 °C. The spectrum of rh-In_2O_3 NCs is also shown for comparison. The spectra were Fourier transformed from *k*-space to *R*-space in the 2.40−10.56 $Å^{-1}$ region. The resulting pseudoradial distribution functions are shown in Figure 7b. The first prominent peak centered at ca. 1.6 Å is due to backscattering of the ejected photoelectron from the first coordination shell of the neighboring oxygen atoms (In−O), while the second peak at ca. 3.0 Å is less pronounced and corresponds to the second shell of cation sites. The inverse Fourier transform of the first (R = 1.0−2.2 Å) and second (R = 2.45−3.60 Å) shells of the pseudoradial distribution functions gives the Fourier-filtered EXAFS spectra, which are shown in Figure S8, Supporting Information. The structural parameters obtained from the first- and second-shell analyses were used as initial parameters for fitting the Fourier-filtered EXAFS spectra (Figure 7c, solid lines), obtained by the inverse Fourier transform of the pseudoradial functions in the full range (R = 1.0−3.6 Å). The Fourier-filtered curves were fit well in the *k*-range of 2.40−10.56 $Å^{-1}$ with two shells (Figure 7c, dashed lines). Table 1 summarizes the structural parameters for the In−O and In−Ga (or In−In) shells obtained from the curve-fitting. For rh-In_2O_3 NCs the fitting results suggest In^{3+} coordination with six oxygen atoms, with an

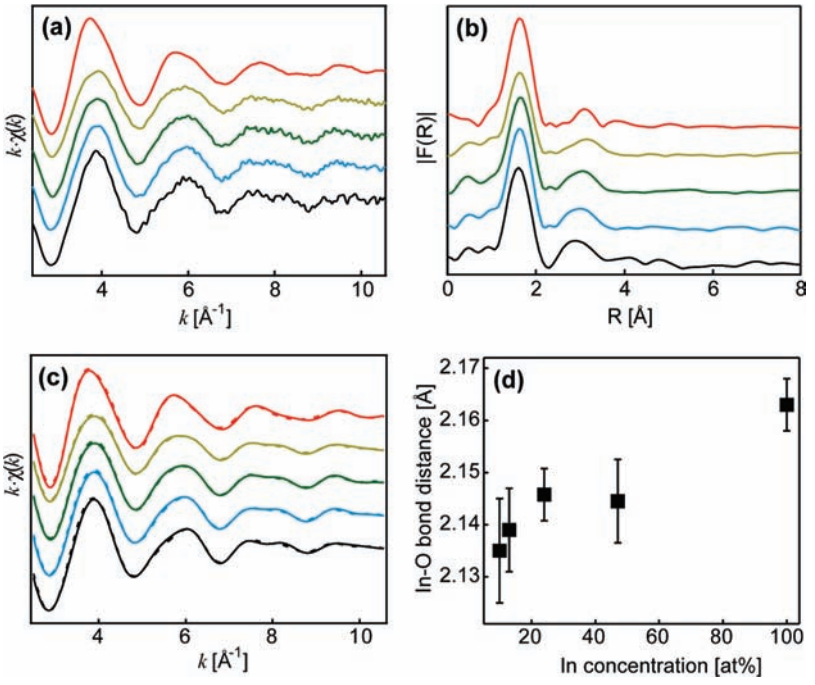

Figure 7. (a) In K-edge *k*-weighted EXAFS spectra of GIO NCs with different compositions synthesized at 200 °C. (b) Pseudoradial distribution functions obtained by Fourier transformation of the spectra in (a). (c) Fourier-filtered EXAFS spectra obtained by the inverse Fourier transform of the radial functions in (b) in the range R = 1.0−3.6 Å (solid lines) and the corresponding curve fits (dashed lines) from which the structural parameters were calculated. (d) In−O bond distances, determined from the EXAFS analysis, as a function of the In concentration in GIO NCs. The spectra in (a)−(c) correspond to In concentrations of 10 (black), 13 (blue), 24 (green), 47 (olive), and 100 (red) atom %.

dx.doi.org/10.1021/ja111514u |*J. Am. Chem. Soc.* 2011, 133, 6711–6719

Table 1. Fitting Parameters Obtained from the Analysis of EXAFS Spectra of GIO NCs Synthesized at 200 °C Having Different In Contents[a]

	In−O			In−Ga			In−In			
[In] (%)	N	R (Å)	σ^2[b] (Å^2)	N	R (Å)	σ^2 (Å^2)	N	R (Å)	σ^2 (Å^2)	ρ[c] (%)
10	5.8	2.135	0.008	4.9	3.053	0.020	0.9	3.356	0.004	0.6
13	5.3	2.139	0.007	2.7	3.063	0.020	1.0	3.349	0.004	0.6
24	5.0	2.145	0.007	2.0	3.051	0.020	1.2	3.330	0.005	0.4
47	4.5	2.144	0.008	0.2	3.040	0.000	1.3	3.343	0.006	0.5
100	6.0	2.163	0.007				2.1	3.252	0.013	0.5

[a] See the Supporting Information for fitting and error analysis equations. [b] Debye−Waller factor. [c] Weighted residual factor.

average In−O bond distance of 2.163 Å. These results are in good agreement with the crystallographic data, from which the average In−O bond length was determined to be 2.17 Å.[37] Metastable γ-Ga_2O_3 has been reported to have a defective spinel-type cubic crystal structure, similar to that of γ-Al_2O_3, with octahedral and tetrahedral cationic sites.[45,46] The majority of Ga^{3+} cations have octahedral coordination, in the ratio $Ga^{3+}(T_d)/Ga^{3+}(O_h) \approx 0.6$.[45,47] The average bond distances for the Ga−O shell in γ-Ga_2O_3 were reported to be 1.88 and 2.00 Å for tetrahedral and octahedral sites, respectively.[47] Understanding the substitutional occupancy of the two sites for different In^{3+} concentrations is, therefore, critical for understanding the optical properties of the complex GIO NCs. EXAFS analysis presented in Table 1 shows that the average In−O bond distances in all GIO NC samples are shorter than those in pure rh-In_2O_3 NCs due to substitution of In^{3+} in γ-Ga_2O_3 or Ga^{3+} in rh-In_2O_3 NCs, both of which result in the reduction of In−O distances. We plotted the In−O bond distances as a function of the In content in GIO NCs in Figure 7d. An increase of In−O bond distances with increasing In concentration in GIO NCs is accompanied by a decrease in the coordination number (N). At a low concentration of In (10 atom %) N is determined to be 5.8, indicating the In^{3+} initially occupies octahedral sites. With increasing concentration of In, N becomes lower, reaching the value of 4.5 at 47 atom % In. This decrease in the coordination number could be due to increased occupancy of the tetrahedral sites by In^{3+} or a local structural disorder due to In^{3+} incorporation and/or a decrease in the NC size. It has been previously reported that in bulk solid solutions In^{3+} substitutes for octahedral Ga^{3+} in β-Ga_2O_3 for In concentrations below 44 atom % at 1000 °C.[48] A further increase in the In concentration upto 95 atom % leads to the formation of both β-Ga_2O_3 and bcc-In_2O_3 phases with different compositions. Above 95 atom % In, Ga^{3+} substitutes for In^{3+} in the bcc-In_2O_3 phase. β-Ga_2O_3 has a monoclinic structure in which half of the Ga^{3+} cations occupy octahedral and the other half tetrahedral sites. This structural consideration in conjunction with the In solubility in bulk β-Ga_2O_3 (44%) indicates that In^{3+} replaces most of the octahedrally coordinated Ga^{3+} sites in β-Ga_2O_3 before undergoing phase separation.[48] The extracted data from EXAFS show a small gradual increase in In−O bond distances for In concentrations below 24 atom % due to incorporation of In^{3+} in the γ-Ga_2O_3 structure (Figure 7d). As the concentration of In approaches that of Ga, the average In−O bond distance becomes nearly constant, although the apparent coordination number still decreases (Table 1). This increase in the average bond distance cannot be explained by the In^{3+} occupation of the smaller tetrahedral sites and is associated with a slight expansion of the Ga_2O_3 NC host lattice with increasing In content. The decrease in the apparent coordination number, N, therefore suggests a distorted local environment around In^{3+}, which can be associated with incorporation of a foreign ion or contribution from the surface sites. At high concentrations of In (above 50 atom %), the In−O bond distances increase again, finally reaching the value for pure rh-In_2O_3.[49] EXAFS results for the second shell support these findings. The coordination number of Ga (N_{In-Ga}) decreases simultaneously with an increase in the coordination number of In (N_{In-In}), indicating substitutional incorporation of In^{3+}. The EXAFS results are in agreement with the XRD results for GIO NCs synthesized at 200 °C. At low concentrations of In only NCs with γ-Ga_2O_3 structure were formed. Upon increasing the concentration of In above 24 atom %, the rh-In_2O_3 phase becomes evident in addition to the γ-Ga_2O_3 phase. From these data we conclude that In^{3+} occupies only octahedral sites in Ga_2O_3 until the saturation limit (ca. 25%) is reached. A further increase in the In precursor concentration leads to the phase segregation and formation of the rh-In_2O_3 phase coexisting with γ-Ga_2O_3. These results are also in agreement with the dependence of the PL energies on the In concentration in GIO NCs (Figure 3c). The emission energy decreases sharply with increasing In concentration up to ca. 30 atom % and then remains unchanged until rh-In_2O_3 becomes the majority phase. It should be noted that the shift of the PL band of GIO NCs with γ-Ga_2O_3 structure is significantly more dependent on the concentration of impurity ions than that of the GIO NCs with rh-In_2O_3 structure. This structural analysis allows for a rational design of complex oxide NCs with targeted photonic properties based on the occupancy of the available crystal lattice sites.

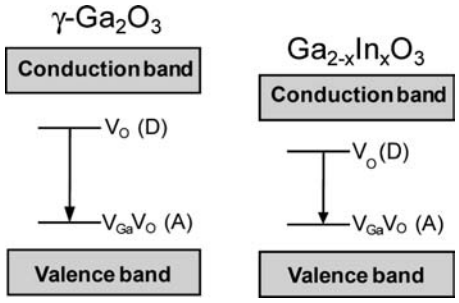

Figure 8. Schematic representation of the possible origin of photoluminescence in undoped γ-Ga_2O_3 NCs (left) and GIO NCs with a γ-Ga_2O_3 structure (right) based on the findings in this work and the evidence previously reported (see the text). The radiative transitions (DAP recombination) are indicated by arrows, and the labels correspond to the defect species described in the text.

Figure 8 schematically depicts the origin of the emission tunability of GIO NCs, on the basis of the results in this work and the previous reports.[5,27,28,50] The blue emission in Ga_2O_3 has been explained by the DAP recombination mechanism, as described above (Figure 8, left). Theoretical work by Maximenko et al.[50] has suggested that recombination of an electron on the localized isoelectronic dopant levels within the band gap with a valence band hole may be a possible source of green emission in Ga_2O_3. The energies of such dopant impurity sub-band gap states are sensitive to the NC composition as well as the band gap width (the incorporation of In^{3+} narrows the band gap, as demonstrated in Figure 3a) and are expected to become lower

dx.doi.org/10.1021/ja111514u |J. Am. Chem. Soc. 2011, 133, 6711–6719

following a decrease in the band gap energy. Another possible explanation for the red shift of the GIO NC emission, and the one favored by the authors of this work, is the changing nature of the DAP recombination with the incorporation of In^{3+} (Figure 8, right). The energy states of the donors and acceptors also follow a reduction in the band gap of GIO NCs, leading to a continuous red shift of the DAP PL band with increased substitutional incorporation of In^{3+}. Furthermore, the average Bohr radius of the donor electrons should also increase with increasing In^{3+} incorporation (i.e., they become more delocalized), favoring faster DAP recombination and a decrease in the delayed PL intensity. The efficiency of the DAP recombination in GIO NCs may be lower than that in pure Ga_2O_3 NCs due to the change in the local environment of the oxygen vacancies or a decrease in the concentration of the gallium and oxygen vacancy sites. This explanation for the red shift of the PL band of GIO NCs would also be consistent with a similar broadening of the PL spectra in Figure 3b.

At a sufficiently high In precursor concentration (>50 atom % with respect to Ga) GIO NCs adopt rh-In_2O_3 structure. However, the origin of PL in In_2O_3 is much less understood. Some literature reports[22] propose that radiative recombination of a photoexcited hole in the valence band with an electron occupying sub-band gap oxygen vacancy states is responsible for the deep-level emission in In_2O_3, similarly to ZnO.[24,25] Other authors suggest the DAP mechanism involving oxygen and indium vacancies,[51] as described above for Ga_2O_3. The PL band shift, broadening, and decay rate for rh-In_2O_3 NCs, as well as the chemical similarity of indium and gallium oxides, are all consistent with the DAP mechanism. The PL in rh-In_2O_3 NCs is, therefore, tentatively also assigned to DAP recombination. It should also be noted that the synthesis conditions and the size of polymorphic NCs play a very important role in determining the defect electronic structure and PL properties. We find that ca. 10 nm bcc-In_2O_3 NCs synthesized at 250 °C are essentially not luminescent (Figure S6, Supporting Information). Weak PL features showing several distinct peaks have been reported for both bcc-[52] and rh-In_2O_3 NCs[53] having similar sizes, synthesized at 290 °C or higher temperatures. These PL transitions have also been attributed to deep energy levels within the band gap, associated with oxygen vacancies. We believe that the higher synthesis temperatures lead to a significantly lower concentration of defect sites in bcc-In_2O_3 compared to rh-In_2O_3 NCs in the present work. While the correlation among the NC phase, defect structure and location, and the observed optical properties of In_2O_3 NCs is beyond the scope of this paper, our results suggest that defect formation in metastable rh-In_2O_3 NCs prepared under the described conditions is more favorable than in bcc-In_2O_3 NCs. Detailed experimental and theoretical investigations of the local environment and electronic structure of the defects responsible for PL in these TCO NCs are currently under investigation.

CONCLUSION

In summary, we demonstrated the structure and composition dependences of the PL properties of colloidal gallium indium oxide NCs. These dependences can be used to achieve a wide tunability of PL in the visible region of the spectrum. The increasing concentration of In in GIO NCs leads to band gap narrowing and a systematic red shift of the PL, which originates from a recombination of an electron trapped on a donor (oxygen vacancy) and a hole trapped on an acceptor (gallium−oxygen vacancy pair). A comparison among the emission energies, efficiencies, and decay rates of γ-Ga_2O_3 and GIO NCs suggests that the emission peak shifts to lower energies with increasing indium content owing to the changes in the energy states of the donors and acceptors and their interactions. EXAFS analysis strongly suggests that In^{3+} is selectively substituted for octahedral Ga^{3+} in metastable γ-Ga_2O_3, which has a spinel-type structure. The changes in the electronic structure of defects, induced by the changes in NC structure and composition, allow for a wide-range tuning of the photoluminescence properties. These defects are also responsible for other functional properties of TCOs, particularly conductivity,[26] and the ability to control both structure and composition lends a new degree of freedom and a path for enhancement of the inherent functionalities of complex TCO NCs. Multifunctionality, achieved in this way, can enable the application of alloyed TCO NCs as integrated optoelectronic materials. One of the envisioned applications of the system described in this work could be in electroluminescent devices.

ASSOCIATED CONTENT

Supporting Information. EXAFS fitting equations, TEM images and XRD patterns of In_2O_3, Ga_2O_3, and GIO NCs, absorption spectra of γ-Ga_2O_3 NCs, PL spectra of γ-Ga_2O_3 and bcc-In_2O_3 NCs, and In K-edge XAS and EXAFS spectra of rh-In_2O_3 and GIO NCs (Figures S1−S8). This material is available free of charge via the Internet at http://pubs.acs.org.

AUTHOR INFORMATION

Corresponding Author
pavler@uwaterloo.ca

ACKNOWLEDGMENT

This work was supported by the Natural Sciences and Engineering Research Council (NSERC) of Canada, Canada Foundation for Innovation, and Canada Research Chairs Program (P.V.R). S.S.F. acknowledges the Waterloo Institute for Nanotechnology for a Graduate Research Fellowship and the Canadian Light Source (CLS) for a Graduate Travel Award. TEM measurements were performed at the Canadian Center for Electron Microscopy in the Brockhouse Institute for Materials Research at McMaster University. XAS measurements described in this paper were performed at the CLS, which is supported by the NSERC, National Research Council, Canadian Institutes of Health Research, and University of Saskatchewan. We thank Drs. Ning Chen and Weifeng Chen (CLS) for their assistance with the XAS measurements and Prof. Eric Prouzet (University of Waterloo) for helpful discussions.

REFERENCES

(1) Cho, K.-S.; Lee, E. K.; Joo, W.-J.; Jang, E.; Kim, T.-H.; Lee, S. J.; Kwon, S.-J.; Han, J. Y.; Kim, B.-K.; Choi, B. L.; Kim, J. M. *Nat. Photonics* **2009**, *3*, 341.

(2) Coe, S.; Woo, W.-K.; Bawendi, M.; Bulovic, V. *Nature* **2002**, *420*, 800.

(3) Achermann, M.; Petruska, M. A.; Kos, S.; Smith, D. L.; Koleske, D. D.; Klimov, V. I. *Nature* **2004**, *429*, 642.

(4) Babinec, T. M.; Hausmann, B. J. M.; Khan, M.; Zhang, Y.; Maze, J.; Hemmer, P. R.; Lončar, M. *Nat. Nanotechnol.* **2010**, *5*, 195.

(5) Vanithakumari, S. C.; Nanda, K. K. *Adv. Mater.* **2009**, *21*, 3581.

(6) Garcia-Santamaria, F.; Miyazaki, H. T.; Urquia, A.; Ibisate, M.; Belmonte, M.; Shinya, N.; Meseguer, F.; Lopez, C. *Adv. Mater.* **2002**, *14*, 1144.
(7) Duan, X.; Huang, Y.; Agarwal, R.; Lieber, C. M. *Nature* **2003**, *421*, 241.
(8) Min, B.; Kim, S.; Okamoto, K.; Yang, L.; Scherer, A.; Atwater, H.; Vahala, K. *Appl. Phys. Lett.* **2006**, *89*, 191124.
(9) Klimov, V. I.; Ivanov, S. A.; Nanda, J.; Achermann, M.; Bezel, I.; McGuire, J. A.; Piryatinski, A. *Nature* **2007**, *447*, 441.
(10) Losev, O. V. *Philos. Mag.* **1928**, *6*, 1024.
(11) Zheludev, N. *Nat. Photonics* **2007**, *1*, 189.
(12) Nag, A.; Sarma, D. D. *J. Phys. Chem. C* **2007**, *111*, 13641.
(13) Bruchez, M., Jr.; Moronne, M.; Gin, P.; Weiss, S.; Alivisatos, A. P. *Science* **1998**, *281*, 2013.
(14) Bawendi, M. G.; Steigerwald, M. L.; Brus, L. E. *Annu. Rev. Phys. Chem.* **1990**, *41*, 477.
(15) Murray, C. B.; Norris, D. J.; Bawendi, M. G. *J. Am. Chem. Soc.* **1993**, *115*, 8706.
(16) Liu, Y.; Koep, E.; Liu, M. *Chem. Mater.* **2005**, *17*, 3997.
(17) Zou, Z.; Ye, J.; Sayama, K.; Arakawa, H. *Nature* **2001**, *414*, 625.
(18) Hamberg, I.; Granqvist, C. G. *J. Appl. Phys.* **1986**, *60*, R123.
(19) Asbury, J. B.; Hao, E.; Wang, Y.; Ghosh, H. N.; Lian, T. *J. Phys. Chem. B* **2001**, *105*, 4545.
(20) Pearton, S. J.; Abernathy, C. R.; Overberg, M. E.; Thaler, G. T.; Norton, D. P.; Theodoropoulou, N.; Hebard, A. F.; Park, Y. D.; Ren, F.; Kim, J.; Boatner, L. A. *J. Appl. Phys.* **2003**, *93*, 1.
(21) Farvid, S. S.; Ju, L.; Worden, M.; Radovanovic, P. V. *J. Phys. Chem. C* **2008**, *112*, 17755.
(22) Liang, C.; Meng, G.; Lei, Y.; Phillipp, F.; Zhang, L. *Adv. Mater.* **2001**, *13*, 1330.
(23) Norberg, N. S.; Gamelin, D. R. *J. Phys. Chem. B* **2005**, *109*, 20810.
(24) Zhang, L.; Yin, L.; Wang, C.; Iun, N.; Qi, Y.; Xiang, D. *J. Phys. Chem. C* **2010**, *114*, 9651.
(25) Vanheusden, K.; Warren, W. L.; Seager, C. H.; Tallant, D. R.; Voigt, J. A.; Gnade, B. E. *J. Appl. Phys.* **1996**, *79*, 7983.
(26) Lorenz, M. R.; Woods, J. F.; Gambino, R. J. *J. Phys. Chem. Solids* **1967**, *28*, 403.
(27) Binet, L.; Gourier, D. *J. Phys. Chem. Solids* **1998**, *59*, 1241.
(28) Wang, T.; Farvid, S. S.; Abulikemu, M.; Radovanovic, P. V. *J. Am. Chem. Soc.* **2010**, *132*, 9250.
(29) Harwig, T.; Kellendonk, F. *J. Solid State Chem.* **1978**, *24*, 255.
(30) Song, Y. P.; Zhang, H. Z.; Lin, C.; Zhu, Y. W.; Li, G. H.; Yang, F. H.; Yu, D. P. *Phys. Rev. B* **2004**, *69*, 075304.
(31) Farvid, S. S.; Dave, N.; Wang, T.; Radovanovic, P. V. *J. Phys. Chem. C* **2009**, *113*, 15928.
(32) Dave, N.; Pautler, B. G.; Farvid, S. S.; Radovanovic, P. V. *Nanotechnology* **2010**, *21*, 134023.
(33) Farvid, S. S.; Dave, N.; Radovanovic, P. V. *Chem. Mater.* **2010**, *22*, 9.
(34) Gill, J. E. *Photochem. Photobiol.* **1969**, *9*, 313.
(35) Michalowicz, A.; Moscovici, J.; Muller-Bouvet, D.; Provost, K. *J. Phys. Conf. Ser.* **2009**, *190*, 012034.
(36) This program can be downloaded from http://leonardo.phys.washington.edu/feff/.
(37) Christensen, A. N.; Broch, N. C.; Heidenstam, O. V.; Nilsson, A. *Acta Chem. Scand.* **1967**, *21*, 1046.
(38) Prewitt, C. T.; Shannon, R. D.; Rogers, D. B.; Sleight, A. W. *Inorg. Chem.* **1969**, *8*, 1985.
(39) Geller, S. *J. Chem. Phys.* **1960**, *33*, 676.
(40) He, H.; Orlando, R.; Blanco, M. A.; Pandey, R.; Amzallag, E.; Baraille, I.; Rerat, M. *Phys. Rev. B* **2006**, *74*, 195123.
(41) Cizeron, J.; Pileni, M. P. *J. Phys. Chem. B* **1997**, *101*, 8887.
(42) Nelson, D. F.; Rodgers, K. F. *Phys. Rev.* **1965**, *140*, A1667.
(43) Dean, P. J. *Prog. Solid State Chem.* **1973**, *8*, 1.
(44) Park, S.; Kwon, J. E.; Kim, S. H.; Seo, J.; Chung, K.; Park, S.-Y.; Jang, D.-J.; Milian Medina, B.; Gierschner, J.; Park, S. Y. *J. Am. Chem. Soc.* **2009**, *131*, 14043.
(45) Kroll, P.; Dronskowski, R.; Martin, M. *J. Mater. Chem.* **2005**, *15*, 3296.
(46) Otero Arean, C.; Lopez Bellan, A.; Penarroya Mentruit, M.; Rodriguez Delgado, M.; Turnes Palomino, G. *Microporous Mesoporous Mater.* **2000**, *40*, 35.
(47) Nishi, K.; Shimizu, K.; Takamatsu, M.; Yoshida, H.; Satsuma, A.; Tanaka, T.; Yoshida, S.; Hattori, T. *J. Phys. Chem. B* **1998**, *102*, 10190.
(48) Edwards, D. D.; Folkins, P. E.; Mason, T. O. *J. Am. Ceram. Soc.* **1997**, *80*, 253.
(49) Although the error bars associated with EXAFS analysis are sizable, the dependence of the In−O bond distance on the In concentration in GIO NCs is very unlikely to be linear, given the comparison of EXAFS with XRD and PL results for the same samples. The linear dependence of the In−O bond distance on the In concentration in GIO NCs would indicate continuous mixing of In and Ga in a single phase, which is not supported by XRD patterns and PL shifts for high In concentrations.
(50) Maximenko, S. I.; Mazeina, L.; Picard, Y. N.; Freitas, J. A., Jr.; Bermudez, V. M.; Prokes, S. M. *Nano Lett.* **2009**, *9*, 3245.
(51) Guha, P.; Kar, S.; Chaudhuri, S. *Appl. Phys. Lett.* **2004**, *85*, 3851.
(52) Liu, Q.; Lu, W.; Ma, A.; Tang, J.; Lin, J.; Fang, J. *J. Am. Chem. Soc.* **2005**, *127*, 5276.
(53) Lee, C. H.; Kim, M.; Kim, T.; Kim, A.; Paek, J.; Lee, J. W.; Choi, S.-Y.; Kim, K.; Park, J.-B.; Lee, K. *J. Am. Chem. Soc.* **2006**, *128*, 9326.